Near-Field Analysis of Surface Waves Launched at Nanoslit Apertures

L. Aigouy*
Laboratoire 'Spectroscopie en Lumière Polarisée', UPR CNRS 5, ESPCI, 10 rue Vauquelin, 75231 Paris Cedex 5, France

P. Lalanne and J. P. Hugonin
Laboratoire Charles Fabry de l'Institut d'Optique, CNRS, Campus Polytechnique, RD 128, 91127 Palaiseau cedex, France

G. Julié and V. Mathet
Institut d'Electronique Fondamentale, UMR CNRS 8622, Bât. 220/221, Université Paris-Sud, 91405 Orsay Cedex, France

M. Mortier
Laboratoire de Chimie de la Matière Condensée de Paris, CNRS, ENSCP 11 rue P. et M. Curie, 75231 Paris Cedex 5, France
(Received 4 October 2006; revised manuscript received 12 January 2007; published 9 April 2007)

With the aim of analyzing the properties of the waves that are scattered by nanoslits on metallic surfaces, we provide a direct observation of the near-field in a slit-doublet experiment at optical wavelengths. We show that two distinct waves are involved: a surface plasmon polariton and another wave with a free-space character. From the recorded data, we have extracted the amplitudes and phases of these waves, their damping characteristic lengths and their relative weights as a function of the separation distance from the slit. The analysis is fully supported by a quantitative agreement with vector-theory computational results.

DOI: 10.1103/PhysRevLett.98.153902 PACS numbers: 42.25.Fx, 42.79.Ag, 73.20.Mf, 78.67.−n

Light transmission from subwavelength apertures has been a subject of long-standing interest in the microwave domain. This interest has been recently renewed at visible frequency by important phenomena such as the extraordinary light transmission [1] or the collimation effect encountered in apertures dressed with subwavelength grooves [2,3]. At a microscopic level, these phenomena are governed by the waves launched by individual nanostructures on the metallic film surface. When created, these waves can interact with other nanostructures to build up the observed phenomena. At optical or near-infrared frequencies, real metals are capable of sustaining modes known as surface plasmon polaritons (SPPs) that are bounded at the interface and readily recognized to mediate the interaction between the nanoapertures [1,2]. With the objective of studying the optical properties of these waves, more elementary structures, composed of a slit and a groove or of two slits, have been studied [4–6]. For large slit separation distances, the observation of an oscillatory transmission as a function of the wavelength of the incident light has unambiguously confirmed the SPPs character of the interaction [4], but for much smaller separation distances like those involved in arrayed nanoapertures, the oscillatory behavior has been shown to strongly differ from that provided by a SPP mode [5–7]. Indeed, the total nearby field scattered on an interface by a nano-object is not a pure SPP and, additionally, incorporates radiative and evanescent field components (REC) [8]. The latter are not bounded at the interface like SPPs, but may creep at the metallodielectric interface over a certain distance and further interact with other nearby nanostructures, just like SPPs.

Many optical phenomena such as the transmissions through arrayed slits or holes, or the oscillatory transmission in slit-doublet experiments, that are observed with metallic nanostructures at visible frequencies, can be reproduced in the THz and microwave domains by scaling the geometrical parameters [9–11]. At these energies, SPPs spread far away into the dielectric medium. Because of their weak confinements, their excitation probability by a subwavelength structure vanishes [12], and they are not involved in the phenomena observed in the long wavelength regime. However, the REC field exists and can be excited at all energies [6]. Despite its importance for conceptual understandings and for applications, its actual characteristics are not well known for noble metals at optical frequencies. In this Letter we provide an accurate description of the field generated by a nanoslit on a metal film. Using a scanning near-field optical microscope (SNOM), we perform a direct visualization of the near field in a slit doublet experiment, and, by anatomizing the fringe pattern, the REC and SPP contributions of each individual slit are extracted. This allows us to analyze their relative amplitudes and phases, and to compare their damping characteristic lengths and their relative weights. In the near infrared, it is found that the REC field is able to propagate over several wavelength distances without significant damping, and that its excitation intensity is as large as the SPP one at subwavelength distances from the slit.

The subwavelength structures are fabricated by electron-beam lithography (FEI XL30S) followed by ion beam etching, in a 100-nm-thick gold layer evaporated onto a fused-silica substrate. The sample consists of a 2D array of slit doublets, with different center-to-center separation

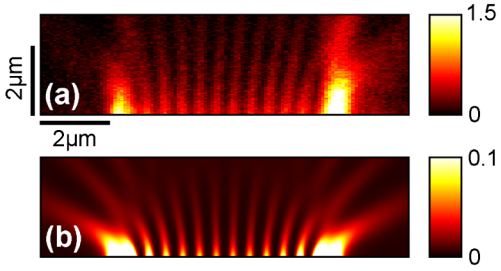

FIG. 1 (color online). Near-field fringe xz pattern in a slit-doublet experiment. (a) Experimental data. (b) Computational results. The displayed image shows $(|E_z|^2 + |E_x|^2)^2$ calculated with a fully vectorial method for the actual parameters measured on the sample and for $2d = 6.24$ μm. The intensity of the images is both saturated at the same level for the sake of clarity.

distances, $2d = 6.24$ and 10.44 μm, and with a 280-nm slit width. For the near-field measurements, the sample is illuminated from the silica substrate by the normally incident beam of a laser diode ($\lambda_0 = 974.3$ nm), polarized in a direction either parallel (TE) or perpendicular (TM) to the slit axes. The SNOM experiments are performed with a subwavelength fluorescent particle settled at the end of a tungsten tip operated in a tapping mode (oscillation amplitude $\sim$10 nm) and placed on a xyz piezoelectric stage for scanning purposes [13]. The particle contains erbium ions that absorb the near-field pattern at λ_0 and fluoresce at visible frequencies (530–550 nm). By collecting the fluorescence as a function of the tip position on the sample, 3D cartographies of the transmitted near-field light are recorded. In contrast to earlier SPP-SNOM experiments [14] that rely on a linear detection scheme, the fluorescence emission involves two-photon absorption, and the recorded images obtained after spectral filtering are therefore expected to scale with $|E|^4$.

In Fig. 1(a), we show the experimental SNOM image obtained for a slit doublet ($2d = 6.24$ μm) in a plane perpendicular to the surface (x, z plane) for TM polarization. The 2D computed image [15] in Fig. 1(b) is performed for a gold permittivity ($\varepsilon_m = -44.05 + 3.24i$) taken from the data in [16]. Essentially, the images evidence the presence of an interference pattern generated by two surface waves, which counterpropagate between the two slits. They represent the near-field part of the Young's fringe pattern generally observed at much larger distances in the far field. Figures 1(a) and 1(b) qualitatively resemble each other: same number of fringes with a dark fringe at the doublet median plane, same hyperbolic fringe rounding in the vicinity of the slits. Figure 2 shows the xy images obtained through horizontal scans of the tip for the same doublet and for the two polarization states. The fringes obtained for TM [Fig. 2(b)] are no longer visible for TE [Fig. 2(a)]. As expected, the amount of surface waves generated for TE is much weaker than for TM because of the different boundary conditions at the air-metal interface for the two polarizations.

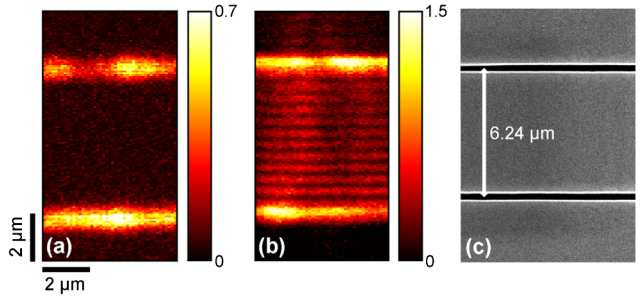

FIG. 2 (color online). yx-scanned near-field images obtained at the air-gold interface of the slit doublet shown in the scanning electron microscope (SEM) photograph (c). The same laser power is used for TE (a) and TM (b) polarizations.

In Fig. 3(a), we present an xy image obtained for the structure with the largest interslit separation distance ($2d = 10.44$ μm). From the recorded pattern we have extracted 10 adjacent horizontal line scans and have further averaged them; see Fig. 3(c). As similarly observed in far-field experiments [5], the near-field interference pattern exhibits two distinct behaviors: a short-range decreasing component with a characteristic length of $\approx$ 2–3 μm, followed by a persistent component with a nearly constant oscillation amplitude in the central part of the structure. We first consider the persistent oscillatory component of the fringe pattern. When they interfere, SPPs offer clear signatures like the associated fringe periodicity $\lambda_{SP}/2 = \pi/\mathrm{Re}(k_{SP})$, where k_{SP} is the SPP propagation constant.

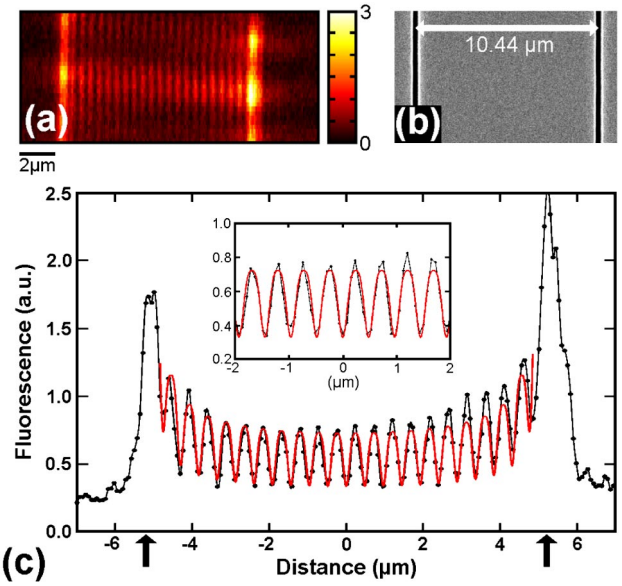

FIG. 3 (color online). (a) xy-scanned near-field image for $2d = 10.44$ μm under TM polarization. (b) SEM picture of the slit doublet. (c) Associated data (black dots) obtained by averaging 10 adjacent line scans from (a). The fitted curve obtained from Eqs. (1) and (2) is shown with the solid red line. The vertical arrows indicate the slit positions. The inset shows the fitted curve obtained for a pure SPP pattern fit in the central part of the interference pattern, $|x| < 2$ μm.

By fitting the oscillations with an offseted-sinusoidal function in the central part of the interference pattern, $|x| < 2\ \mu$m in Fig. 3(c), the fringe spacing is determined to be equal to 480.5 nm $\pm$ 2 nm. Compared to the SPP half-wavelength computed from the data in [16], $\lambda_{SP}/2 = 481.1$ nm, the relative deviation is as weak as 0.12%. This evidences that the REC field is negligible at slit distances larger than $3\lambda_0$, and that the launched surface wave is there mainly composed of a SPP.

In order to access to the main characteristics of the REC field, we further provide an in-depth analysis of the recorded near-field data. The analysis is rendered difficult because of the presence of spatial uniformities, of eventual noise, and of an inevitable contamination of the actual near field by the tip. However, as we shall see, it is possible to extract the main REC-field properties with a few reasonable assumptions that will be further checked by comparison with fully vectorial computational results. First, we assume that the recorded near-field pattern results solely from the interference of two counterpropagating waves scattered on the interface by the slit apertures ($x = \pm d$), and that each wave is a superposition of a background SPP mode and of a REC field. Therefore, the total magnetic field on the interface ($z = 0$) between the slits reads as $H_y = H_c(x-d) + H_{SP}(x-d) + H_c(x+d) + H_{SP}(x+d)$, where H_{SP} refers to the SPP mode and H_c to the REC field. H_{SP} is known analytically but no closed form expression exists for H_c in the literature. In general, the latter can be written as a superposition of homogeneous and inhomogeneous plane waves, whose respective weights depend on the geometrical parameters of the scatterer and on the dielectric properties of the interface [6]. To remove the absence of theoretical results, we further assume that H_c takes the approximate form $H_c(x) \propto \exp(ik_0x)/x^{1/2}$, k_0 being the free-space wave vector modulus. The cylindrical-wave approximation is virtually exact in the limit of infinitively small scatterers (line source) on a perfectly conducting plane [6], and is expected to remain qualitatively valid for nanoslits in a real metal film at small distances from the slit [17]. Finally, we assume that, as it is the case for the SPP modes, the z component $E_{z,C}$ of the REC electric field is dominant and we neglect the contribution of the other x component ($|E_{z,C}| \gg |E_{x,C}|$). Under these assumptions, the signal $S(x)$ emitted by the fluorescent particle and detected in the far field is simply

$$S(x) \propto \int_{x-a/2}^{x+a/2} |E_z(u)|^4 du, \tag{1}$$

with

$$E_z = A_{SP}\exp(ik_{sp}d)\sin(k_{SP}x) + A_c\frac{\exp[ik_0(x+d)]}{(x+d)^{0.5}} \times\left[ik_0 - \frac{0.5}{(x+d)}\right] - A_c\frac{\exp[-ik_0(x-d)]}{(d-x)^{0.5}} \times\left[ik_0 - \frac{0.5}{(d-x)}\right]. \tag{2}$$

In Eq. (2), A_{SP} is a scalar, and A_c is a complex number whose argument accounts for a possible phase delay between the SPP modes and the REC fields. The convolution by a window of length a in Eq. (1) results from the spatial integration due to the finite fluorescent particle size. In Eqs. (1) and (2), A_{SP}, A_c, and a are unknown parameters to be optimized by fitting the processed data. To calculate these coefficients, we adopt a two-step procedure. We first consider the central part of the interference pattern, and under the assumption (*a posteriori* verified) that the near field is solely composed of two counterpropagating SPPs there, $|A_c| \ll |A_{SP}|$; we find that $A_{SP} = 1.45$ and $a = 0.38\ \mu$m from the fitted curve shown in the inset of Fig. 3(c). The a value is in good agreement with the 0.4 μm average size of the fluorescent particles used in the experiments. In a second step, using Eq. (2) with A_{SP} and a fixed to their optimized values, we fit the experimental data over the full spatial interval between the slits. As shown in Fig. 3(c), a good agreement is obtained between the experimental data (black circles) and the fitted curve (solid red line) evaluated for the optimized parameter, $A_c = -0.014 + 0.046i$.

From the previous analysis, we now investigate the optical properties of the near-field waves launched by an isolated nanoslit at a metallic interface. According to Eq. (2), the z component E_z of the electric field reads as

$$E_z(x_s) = E_{z,SP}(x_s) + E_{z,C}(x_s) = \frac{A_{SP}}{2i}\exp(ik_{sp}x_s) + A_c\frac{\exp(ik_0x_s)}{x_s^{0.5}}\left[ik_0 - \frac{0.5}{x_s}\right]. \tag{3}$$

Using Eq. (3) with the fitted parameters, we have represented the real parts of E_z, $E_{z,SP}$, and $E_{z,C}$ as a function of the slit distance x_s; see Fig. 4(a). Clearly, these data and Eq. (3) rely on a number of approximations and need to be cross-checked. For that purpose, we have calculated [15] the field scattered by an isolated slit, for parameters identical to those used in the doublet experiment. From the total field calculated on the rear air side of the slit, we have separated the SPP and REC-field contributions by applying the formalism developed in [12], and have further adjusted the complex amplitude of the incident wave so that the calculated value of the total field E_z exactly matches that obtained with Eq. (3) at $x_0 = 8\ \mu$m. The computed data are displayed in Fig. 4(b). An overall good agreement, especially for the relative phase difference between $E_{z,SP}$ and $E_{z,C}$, is achieved with the data of Fig. 4(a). There are also some differences. Clearly, the experimentally driven data underestimate the initial REC intensity and also predict a slight initial phase shift between the REC field and the SPP, while the computational data show that, indeed, the two waves are exactly excited in phase. We believe that these discrepancies result from the fact that, when positioned in the close vicinity of a slit, the fluorescent particle cannot be considered as completely passive. It probably

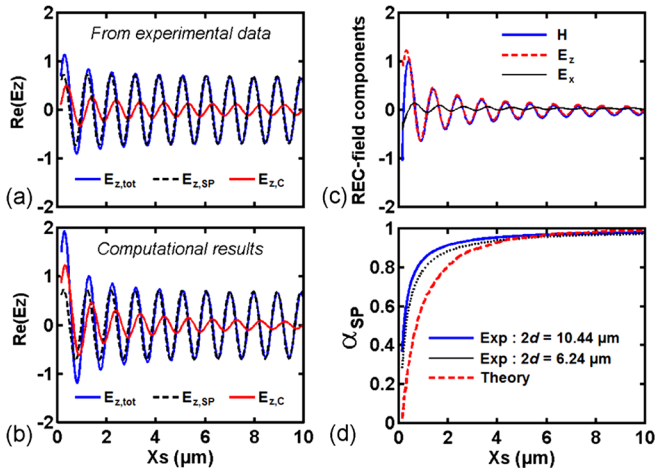

FIG. 4 (color online). REC-field main characteristics and comparison with fully vectorial computational results. (a) and (b) Real part of the electric-field z component scattered by an isolated nanoslit on an interface as a function of the separation distance x_S from the slit center : SPP (black-dashed line), REC field (red-thick line), total field (blue line). (a) Extracted with Eq. (3) from the experimental data. (b) Computational results displayed with the same scale. (c) Calculated REC-field components as a function of x_S: Re(H_C) in blue, Re($E_{z,C}$) in red-dashed and Re($E_{x,C}$) in black. (d) Relative fraction α_{SP} of the intensity carried by the SPP mode. The red-dashed curve corresponds to computational results. The black-dotted and blue-solid curves are obtained from Eq. (3) with the optimized fitted parameters for $2d = 6.24$ and 10.44 μm, respectively.

perturbs the scattered field that cannot be fully recovered at subwavelength distances. Figure 4(c) shows computational results obtained for the three components, $H_{y,C}$ (blue), $E_{z,C}$ (red), and $E_{x,C}$ (black), of the REC field on the interface. Consistently with the cylindrical-wave approximation, all components exhibit a near free-space oscillatory wave with a quadrature phase shift between $E_{z,C}$ and $E_{x,C}$. Additionally, and consistently with our previous approximation, $|E_{z,C}|$ is found to be much larger than $|E_{x,C}|$. Finally, in Fig. 4(d), we show the SPP relative intensities, $\alpha_{SP} = |E_{z,\mathrm{SP}}|^2/(|E_{z,\mathrm{SP}}|^2 + |E_{z,C}|^2)$, as a function of the slit separation distance. Again, the experimentally driven data obtained for $2d = 10.44$ μm (blue-solid line) and for $2d = 6.24$ μm (black-dotted line) agree well with the computational data (red-dashed line). Because of their different damping characteristics, the REC-field decay rate is much faster than the SPP one, and for $x_s > 2\lambda$, at least 80% of the energy propagated at the interface is carried by the SPP. Equally importantly, the initial excitations of the two waves are found to be almost equal for subwavelength distances.

In conclusion, computational and near-field experimental data have both evidenced that the waves launched by a single nanoslit on a metallodielectric interface are a combination of two different near-field contributions: a bound SPP mode with a classical exponential damping characteristic and another field with nearly free-space cylindrical-wave characteristics. Although more studies are needed for full assessment, especially for nanoholes that do not sustain propagative modes, we believe that the two-wave model picture represents a helpful microscopic picture for the physics and for the engineering of many recent phenomena involving multiple scattering by arrayed subwavelength apertures in perforated metal films. At visible frequencies, the interaction between the apertures is mainly mediated by SPPs. In the long wavelength limit, this is no longer the case and the REC field dominates. The latter is excited with approximately the same initial phase and intensity as the SPP ones in the visible and it propagates with almost the same phase velocity. All these similarities might well explain why some important phenomena encountered at visible frequencies [1–4] also occur at much longer wavelengths [9–11].

The authors are grateful for support from the Conseil Général de l'Essonne through the use of the equipments of the CTU IEF-MINERVE.

*Electronic address: aigouy@optique.espci.fr

[1] T. W. Ebbesen *et al.*, Nature (London) **391**, 667 (1998); W. L. Barnes *et al.*, Nature (London) **424**, 824 (2003).
[2] H. J. Lezec *et al.*, Science **297**, 820 (2002).
[3] F. J. García-Vidal *et al.*, Phys. Rev. Lett. **90**, 213901 (2003).
[4] H. F. Schouten *et al.*, Phys. Rev. Lett. **94**, 053901 (2005).
[5] G. Gay *et al.*, Nature Phys. **2**, 262 (2006).
[6] P. Lalanne *et al.*, Nature Phys. **2**, 551 (2006).
[7] L. Chen *et al.*, Opt. Express **14**, 12 629 (2006).
[8] A. Banos, *Dipole Radiation in the Presence of a Conducting Half-Space* (Pergamon, New York, 1966); At optical frequencies, see for instance, F. Pincemin *et al.*, J. Opt. Soc. Am. A **11**, 1117 (1994).
[9] J. Gómez Rivas *et al.*, Phys. Rev. B **68**, 201306(R) (2003).
[10] R. Gordon, J. Opt. A Pure Appl. Opt. **8**, L1 (2006).
[11] F. J. G. de Abajo *et al.*, Opt. Express **14**, 7 (2006).
[12] P. Lalanne *et al.*, Phys. Rev. Lett. **95**, 263902 (2005).
[13] L. Aigouy *et al.*, Appl. Phys. Lett. **83**, 147 (2003).
[14] A. Bouhelier *et al.*, Phys. Rev. B **63**, 155404 (2001); L. Yin *et al.*, Appl. Phys. Lett. **85**, 467 (2004); J. C. Weeber *et al.*, Phys. Rev. B **70**, 235406 (2004); Z. Liu *et al.*, Nano Lett. **5**, 1726 (2005); H. Gao *et al.*, Nano Lett. **6**, 2104 (2006).
[15] E. Silberstein *et al.*, J. Opt. Soc. Am. A **18**, 2865 (2001).
[16] E. D. Palik, *Handbook of Optical Constants of Solids* (Academic, New York, 1985), Part II(1).
[17] For real metals, the REC field at the metallodielectric interface additionally experiences the metallic finite conductivity. This results in a more intricate damping behavior, as shown from asymptotic studies in the limit of infinitely small apertures [6].